

Total-energy-based prediction of a quasicrystal structure

M. Mihalkovič,^{1,2} I. Al-Lehyani,³ E. Cockayne,⁴ C. L. Henley,⁵ N. Moghadam,⁶ J. A. Moriarty,⁷ Y. Wang,⁸ and M. Widom³

¹*Institute für Physik, Technische Universität Chemnitz, D-09107 Chemnitz, Germany*

²*Institute of Physics, Slovak Academy of Sciences, Bratislava, Slovakia*

³*Department of Physics, Carnegie Mellon University, Pittsburgh, Pennsylvania 15213*

⁴*Ceramics Division, NIST, Gaithersburg, Maryland 20899-8520*

⁵*Department of Physics, Cornell University, Ithaca, New York 14853*

⁶*Oak Ridge National Laboratory, Oak Ridge, Tennessee 37831-6114*

⁷*Lawrence Livermore National Laboratory, Livermore, California 94551*

⁸*Pittsburgh Supercomputer Center, Pittsburgh, Pennsylvania 15213*

(Received 9 October 2001; published 1 March 2002)

Quasicrystals are metal alloys whose noncrystallographic symmetries challenge traditional methods of structure determination. We employ quantum-based total-energy calculations to predict the structure of a decagonal quasicrystal from first-principles considerations. Our Monte Carlo simulations take as input the knowledge that a decagonal phase occurs in Al-Ni-Co near a given composition and use a limited amount of experimental structural data. The resulting structure obeys a nearly deterministic decoration of tiles on a hierarchy of length scales related by powers of τ , the golden mean.

DOI: 10.1103/PhysRevB.65.104205

PACS number(s): 61.44.Br, 61.43.Bn, 61.50.Lt, 61.66.Dk

I. INTRODUCTION

Al-Ni-Co forms thermodynamically stable and highly perfect decagonal quasicrystalline samples over a range of compositions.¹ Of special interest is the composition $\text{Al}_{0.70}\text{Ni}_{0.21}\text{Co}_{0.09}$ for which the structure is periodic along the z axis with a period of $c = 4.08 \text{ \AA}$, and quasiperiodic perpendicular to this axis with a characteristic length (termed a “quasilattice constant”) of $a_0 = 2.45 \text{ \AA}$.² This “basic Ni” composition is well suited for theoretical modeling because it should be the simplest structure, lacking the quasiperiodic modulation and c -axis doubling observed at other compositions. Numerous attempts to determine the structure of this compound start from experimental data^{3–7} but do not *predict* a structure on the basis of total energy.

The transition metals Ni and Co (generically denoted TM) play similar chemical roles in Al transition-metal quasicrystals, and they are not distinguished by ordinary x-ray or electron diffraction. In contrast, we distinguish Ni and Co in this work, treating Al-Ni-Co as a ternary system.

Our work employs total-energy calculations based on pair potentials derived from first-principles electronic structure considerations. Monte Carlo simulations are used to find favorable atomic decorations and tiling structures. The *existence* of a tenfold symmetric stable phase, and the lattice constants of that phase are taken as experimental input. The pair potentials, experimental input, and Monte Carlo methods are described in Sec. II below.

Using these methods we find low-energy structures can be described using nearly deterministic decorations of rigid tiles. Specific features of the pair potentials are responsible for certain details of the structure over short length scales, as we describe in Sec. III A. Taking decorated tiles as fundamental objects, we then perform larger-scale simulations and find an alternate structural description (see Sec. III C) in

terms of tiles whose edge length is a factor of τ^2 larger [$\tau = (\sqrt{5} + 1)/2$ is the golden mean]. Details of our structural model are compared with experimental data in Sec. IV.

II. METHODS

Our total-energy calculations employ quantum-based pair potentials derived from the generalized pseudopotential theory (GPT).⁸ GPT expands the total energy in a series of volume, pair, and many-body potentials. The volume term exerts no force and may be neglected at fixed volume and composition. The many-body terms are small except among clusters of neighboring transition-metal atoms, and we incorporate their influence with modified short-range TM-TM pair interactions constrained by full *ab initio* calculations.⁹

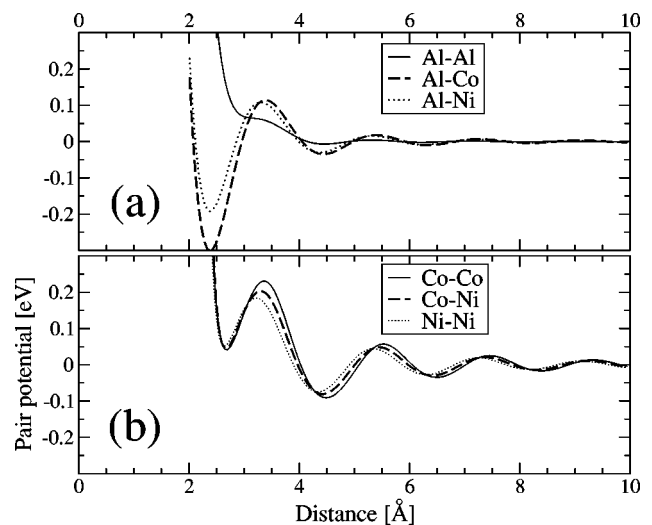


FIG. 1. (a) GPT pair potentials for Al-Al, Al-Co, and Al-Ni. (b) Modified GPT pair potentials for Co-Co, Co-Ni, and Ni-Ni.

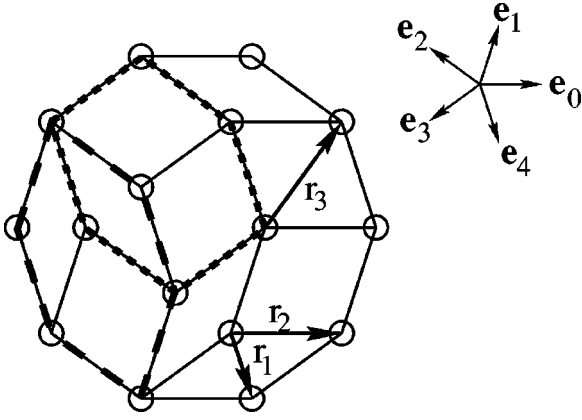


FIG. 2. Random rhombus tiling decorated with ideal sites. The long- and short-dashed lines outline, respectively, thin and fat hexagons. Unit vectors $\{\mathbf{e}_i\}$ lie parallel to tile edges. Vectors \mathbf{r}_i are defined in Table I.

Figure 1 displays the resulting pair potentials.^{8,9} Note that they oscillate with a spatial frequency that asymptotically approaches $2k_F$, with k_F the Fermi wave vector. Compatibility of atomic separations with minima of the oscillating potentials can lower the total energy. This can be shown using second-order perturbation theory within the independent electron approximation when $2k_F = |\mathbf{G}|$, with \mathbf{G} a reciprocal-lattice vector. This is one of the Hume-Rothery mechanisms for structural stability. For our simulations we cut off the potential using a smooth truncation on the interval from 8 to 10 Å.

We identify four salient short-range properties of the pair potentials: (1) $V_{\text{AlAl}}(r)$ has a broad shoulder starting around $r = 2.9$ Å and is repulsive at shorter distances, (2) $V_{\text{AlCo}}(r)$ and $V_{\text{AlNi}}(r)$ exhibit deep first minima near $r = 2.5$ Å and second minima near $r = 4.5$ Å, (3) the V_{AlCo} well is significantly deeper than the V_{AlNi} well, and (4) the modified $V_{MM}(r)$ have shallow minima near $r = 2.6$ Å.

The following features of the $d(\text{AlNiCo})$ structures are evident in the experimentally determined Patterson function^{3,7} which contains a peak at every interatomic vector \mathbf{r} : (A) All atoms lie on or nearly on layers separated by $c/2 = 2.04$ Å, (B) the vector from an atom to a nearest neighbor (with a tolerance of ~ 0.1 Å) belongs to a small, discrete basis set of “linkage” vectors, and (C) the in-plane components of linkage vectors are $\pm a_0 \mathbf{e}_i$ (see Fig. 2) or simple sums of such vectors.

TABLE I. Characteristic distances (illustrated in Fig. 2) and important bond types. Primed vectors connect adjacent layers.

Label (Å)	Example	Comment
$r_1 = 1.51$	$a_0(\mathbf{e}_0 + \mathbf{e}_3)$	forbidden
$r_2 = 2.45$	$a_0 \mathbf{e}_0$	Al-M, (Al-Al)
$r'_1 = 2.54$	$a_0(\mathbf{e}_0 + \mathbf{e}_3) + \frac{c}{2} \hat{z}$	Al-M, M-M
$r_3 = 2.88$	$a_0(\mathbf{e}_1 - \mathbf{e}_0)$	Al-Al
$r'_2 = 3.19$	$a_0 \mathbf{e}_0 + \frac{c}{2} \hat{z}$	Al-Al

We construct trial quasicrystal structures that achieve low total energy while satisfying the above experimental constraints. To enforce constraints (B) and (C) we limit atomic positions to a collection of discrete sites (Fig. 2), located at vertices of a two-dimensional tiling of rhombi with edges a_0 and acute angles 36° or 72° . To enforce constraint (A) we stack two independent tilings above each other. As the tiles can be placed in many ways, and atoms distributed randomly among the sites, these *minimal constraints* permit a great variety of structures, including all reasonable quasicrystal structures. After we discover favorable low-energy motifs consistent with the minimal constraints, we remove unnecessary degrees of freedom, effectively defining *highly constrained* models.

Metropolis Monte Carlo annealing, in which the temperature is reduced slowly in discrete steps, yields low-energy structures. Care is taken to anneal for long times at those intermediate temperatures where significant degrees of freedom begin to freeze. Two kinds of Monte Carlo steps are employed: (i) swaps between nearby atoms (within 6 Å) of different species in either layer, including hops of one atom to an empty ideal site nearby and (ii) “flips” (in one layer) which reshuffle the three rhombi in a fat or thin hexagon (both types of hexagon are shown in Fig. 2). Due to the hexagon flips, our ensemble is an “equilibrium random tiling” allowing phason disorder,¹⁰ but the system is free to find a unique state if that is favored by the potentials. Our simulations are performed with periodic boundary conditions using cell sizes chosen to best approximate the quasiperiodic structure. Additional simulation details are given in Sec. III. Note that certain Monte Carlo steps of type (i) (atom swaps) are prohibited in some of our nearly deterministic decoration simulations.

III. RESULTS

A. Local order from minimally constrained simulation

In our initial simulation with minimal constraints, we employ a cell of size $12.22 \times 14.37 \times 4.08$ Å³ and composition $\text{Al}_{34}\text{Ni}_{12}\text{Co}_4$. This cell contains 72 ideal sites, 36 in each layer with the c -axis periodicity enforced. We cool slowly starting from a random high-energy configuration. Our initial annealing is carried out at very high temperature ($\beta \equiv 1/k_B T = 0.5$ eV⁻¹, $T = 23\,208$ K), with the temperature dropping eventually to near room temperature ($\beta = 35.0$ eV⁻¹, $T = 332$ K). This protocol identifies a unique minimum-energy configuration illustrated in Fig. 3(a).

The optimal configuration can be described simply in terms of a new *highly constrained* model [see Fig. 3(b)] that obeys the following rules: (i) the entire plane is tiled by three compound tiles called “hexagon,” “boat,” and “star” (HBS), outlined by heavy edges and built respectively of three, four, and five rhombi (this is called the “HBS” tiling¹¹). (ii) The optimal decoration of the HBS tiles is virtually unique. Minimally constrained simulations with larger cells support these rules.

We can understand this decoration in terms of the salient features of the potential we enumerated at the start. In view of features (1) and (2), the minimum-energy structure must

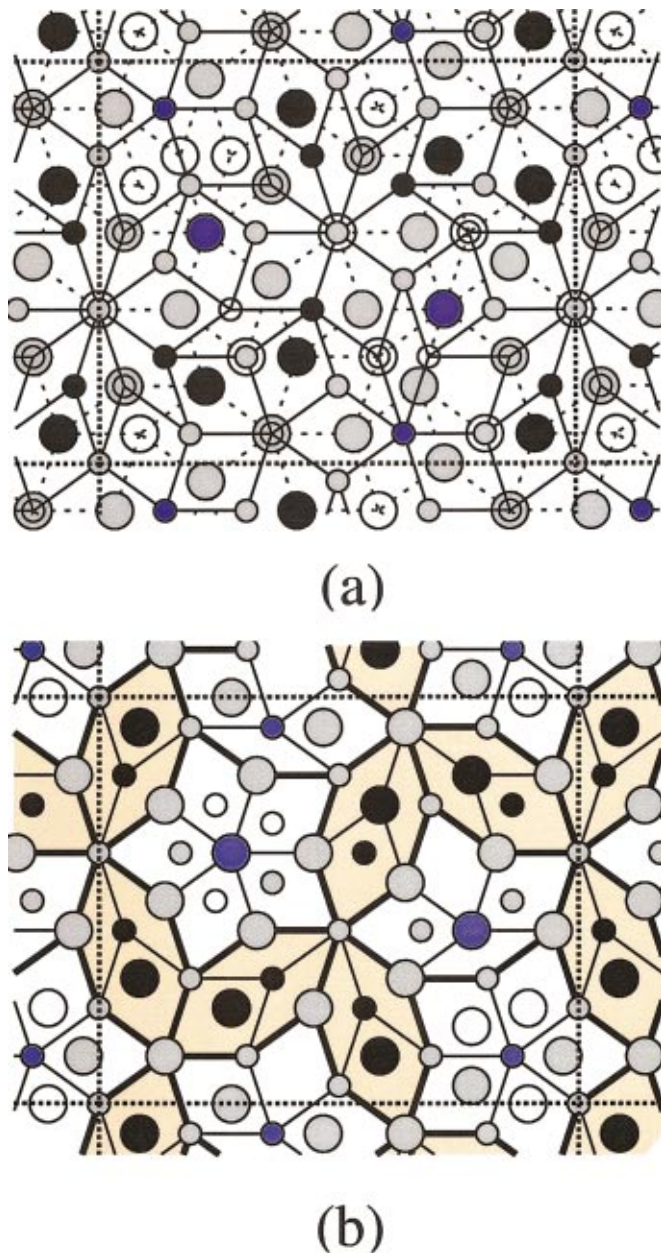


FIG. 3. (Color) Minimum-energy configurations. Small/large circles indicate atoms in upper/lower layers. Gray=Al, blue=Co, black=Ni, and white=vacant. (a) Top figure results from minimally constrained simulation (solid/dashed lines denote upper/lower tilings). (b) Bottom figure results from highly constrained simulation. Dark solid lines outline a_0 -scale HBS tiling. Shaded hexagons connect vertices of $\tau^2 a_0$ -scale HBS tiling.

maximize the number of Al-Co and Al-Ni bonds. In view of feature (3), every Co ought to have purely Al neighbors, which is geometrically feasible just up to $\sim 10\%$ Co, which is the “basic” composition. Thus, all TM-TM neighbors must be Ni-Ni. Every Ni has mostly Al neighbors but cannot escape having two or three Ni neighbors, since $\sim 30\%$ of all atoms are transition metals.

Let us check which ideal-site separations are favorable for which atom pairs. Within the same layer, the tile edge length $r_2 = 2.45 \text{ \AA}$ is unfavorable for Al-Al or TM-TM bonds, but

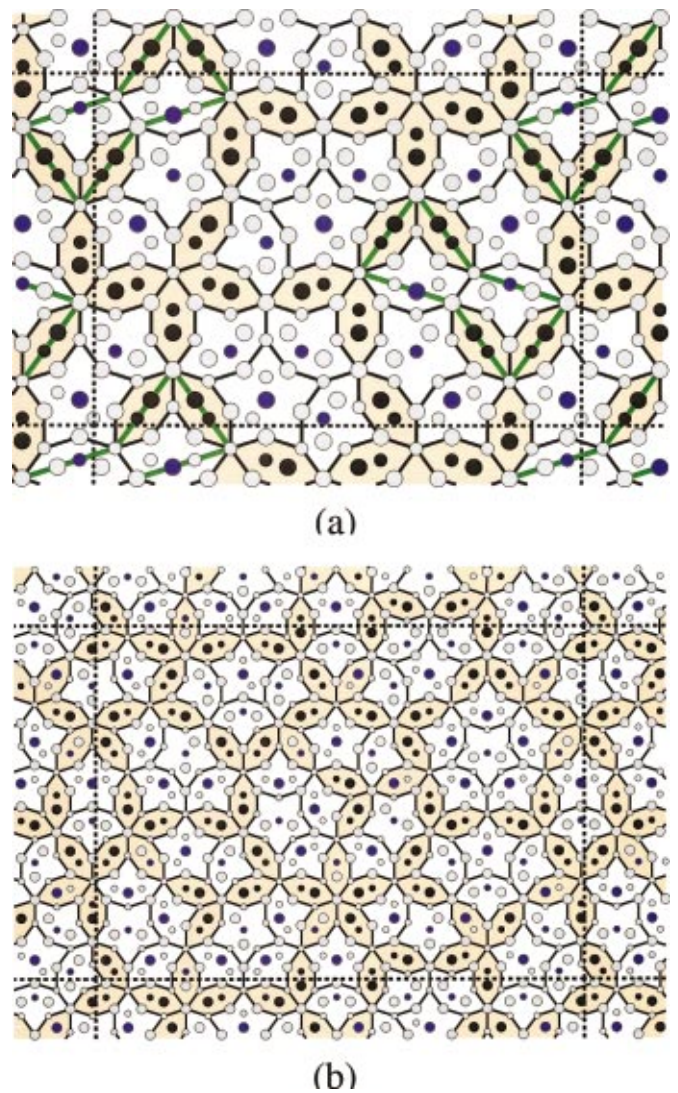


FIG. 4. (Color) Lowest-energy configurations obtained. (a) Top shows highly constrained simulation. Green lines outline bow-tie tiles. (b) Bottom shows variable occupancy simulation. Small hexagonal tiles, occupied by either NiNi pairs or AlCo pairs, lie on edges of an HBS supertiling in (b).

highly favorable for Al-TM bonds. However, because of the high density of Al atoms, we find a small number of Al-Al bonds do take this length. The short diagonal of a fat rhombus is $r_3 = 2.88 \text{ \AA}$, which is an acceptable Al-Al distance. Hence the 72° Al-TM-Al isosceles triangle (half a fat rhombus) is highly favored within a layer.

The interlayer spacing $c/2 = 2.04 \text{ \AA}$ is too short for any pair. Sites in adjacent layers, spaced by $\tau^{-1} a_0$ in-plane (e.g., the short diagonal of the thin rhombus), are separated by $r'_1 = 2.54 \text{ \AA}$ which is favorable for Al-TM or TM-TM bonds. Finally, sites in adjacent layers separated by a_0 in plane have a total separation of $r'_2 = 3.19 \text{ \AA}$ which is an acceptable Al-Al distance.

Given this understanding of chemical bond lengths we can easily justify the decoration of the HBS tiles. Each tile is bounded by Al atoms of alternating heights at separation r'_2 . Interior sites of the hexagon tile are too close to the Al bor-

der for Al atoms. Since it must hold two TM atoms, it holds a pair of Ni atoms at distances r'_1 and r_2 from the border Al and mutual separation r'_1 . Four of the border Al atoms form a rectangle with edges r'_2 and r_3 lying in a plane that is nearly the perpendicular bisector of the Ni-Ni bond. This fragment of the hexagon tile is thus a slightly distorted region of $B2$ (CsCl) structure.¹²

The interior vertex of the boat and star tiles are at the ideal TM distance r_2 from border Al atoms. Since this is a point of high Al coordination, it is occupied by Co. The boat and star tiles have room for two additional interior Al atoms at separation r_3 . In an isolated star tile this interior Al pair can lie in any of five symmetry-related configurations. The structure surrounding the star generally breaks this degeneracy by means of long-range interactions.

In the decoration just described, an Al atom on an HBS tiling vertex is often at the center of a small cluster which was an important motif of earlier models^{11,13} and is confirmed by x-ray structure refinement.⁶ This cluster appears in Fig. 3(b) wherever hexagons join at their tips. This cluster consists of a pentagon of mixed Al and Ni atoms in the same layer as the vertex Al, and additional pentagons in the adjacent layers above and below. These adjacent pentagons contain only Al atoms and are rotated by 36° with respect to the middle pentagon. This cluster exhibits interlayer Al-Ni separations of 2.54 Å and 4.46 Å, precisely at the first and second minima of V_{AlNi} .

Since the HBS tile corners are all multiples of 72° , edges emanating from the HBS corner atoms in one layer can only point in the five directions $+\mathbf{e}_i$ while those within the other layer point in the directions $-\mathbf{e}_i$. Statistically, the layers are equivalent but related by a screw axis. Allowing for the reflection planes normal to the layers, and in the absence of further symmetry breaking, the HBS decoration implies a space group $10_5/mmc$, consistent with experiment.

B. Highly constrained simulation

For the next level of modeling, we take the highly constrained HBS tiles as fundamental objects. Tile-tile interactions are defined implicitly as the sum of the pair potentials between atoms decorating the tiles. The allowed “flips” (Monte Carlo moves) of the HBS tiling are called “bow-tie flips” as the tile edges before and after the flip outline a bow-tie shape.¹¹ The bow-tie flips are generated by fat hexagon flips of the underlying rhombus tiling. Additionally the Al pair inside the star can rotate among its five allowed orientations. The reduced degrees of freedom make the highly constrained HBS tiling much faster to simulate at low temperatures than the minimally constrained rhombus tiling.

The ensemble of random HBS tilings contains a variable tile frequency ratio H:B:S because HS pairs interchange with BB pairs by bow-tie flips. Highly constrained simulations forbid this flip because it alters the chemical composition, given our ideal tile decoration. There is a particular “golden” ratio H:B:S = $\sqrt{5}\tau:\sqrt{5}:1$ that is obtained, for example, by removing double-arrow edges from a Penrose tiling. Decorating such a tiling deterministically yields an ideal composition $\text{Al}_{0.700}\text{Ni}_{0.207}\text{Co}_{0.093}$ and atomic volume 14.16 Å³. The

composition is consistent with experiment, while the atomic volume is low by about 5%.^{6,7} The real structure probably incorporates partial occupancy and is less strictly decorated than this model.

C. Supertiling

Large-scale simulations (see Fig. 4) reveal a “supertile” ordering in which hexagons connect tip to tip. Each hexagon tip becomes a vertex of a “supertiling,” with longer edges of length $\tau^2 a_0$ along the midline of every hexagon. Since orientations of adjoining hexagons differ by multiples of 72° , the same is true for their midlines, hence the “supertile” edges differ by 72° angles and form mainly HBS tiles (as well as a new “defect” tile discussed below). Each HBS supertile has Al atoms at its vertices, Ni atom pairs along its edges, and Al and Co atoms at special points in its interior. The only variability in the supertile decoration occurs in the asymmetric placement of one (in H and B) or two (in S) interior Al atoms.

The supertile atomic structure is mechanically stable. Under relaxation of the structure shown in Fig. 3 (which consists of two large-scale hexagons), the average Co and Ni displacement is just 0.10 Å. The average Al displacement is 0.17 Å except for the two Al atoms located slightly off center in the large-scale hexagons which displace 1.13 Å to the symmetric points at the hexagon centers.

The energetics of the HBS supertilings follows a “tile Hamiltonian” in which we replace the actual interatomic interactions with effective interactions within and between the tiles. The tiles are decorated deterministically as in Fig. 4(a). The functional form

$$H = c_0 N_{\text{atoms}} + c_{72} N_{72} + c_{144} N_{144} \quad (1)$$

provides a reasonably simple and accurate description. Here N_θ is the number of vertices of angle θ . We obtained energy data from a Monte Carlo simulation at $k_B T = 0.1$ eV during which we monitored the energies of 1400 accepted flips of an $L_x \times L_y \times 4$ Å³ approximant structure containing 1466 atoms in its unit cell. The resulting coefficients are $c_0 = -0.246$ eV, $c_{72} = 0.218$ eV, $c_{144} = -0.056$ eV, and the rms deviation of the actual energies from this fit is 0.021 eV. Of this deviation, we account for 0.007 eV simply from the placement of symmetry-breaking Al atoms in the supertile interiors.

Note that 72° angles are disfavored ($c_{72} > 0$) because they increase the number of NiNi neighbors and thereby reduce the number of favorable Al-Ni neighbors. Flips of the supertiling that replace an HS pair with a BB pair result in a net reduction of one 72° angle. Thus low-energy structures of the HBS supertiling contain few or no S tiles. Our Hamiltonian depends only on the numbers of tiles of each type and contains no interactions between tiles. Consequently it has a highly degenerate ground state. A more accurate Hamiltonian would contain some weak terms that couple to the arrangement of the tiles. Additionally, we do not include stacking disorder. A large term should be added to Eq. (1) to model the energy cost of a mismatch in the tiling between successive 4 Å slabs.

The “defect” tile, with a shape we call a “bow tie,” breaks the connectivity of the small-hexagon chain. Defect tiles enter only when they reduce the number of 72° junctions. They accomplish this reduction by interchanging a Ni-Ni pair with a nearby Al-Co pair. We can include the defect in our tile Hamiltonian by adding an additional term $c_{\text{defect}}N_{\text{defect}}$ with $c_{\text{defect}}=0.020$ eV. Despite the positive sign of this term, defects lower the total energy by virtue of a reduction in N_{72} .

An alternate means of reducing the frequency of 72° angles between tile edges decorated with Ni atom pairs is to alter the chemical composition. To accommodate the new composition we must relax certain constraints in our simulation. We keep the small-scale HBS tiles with Al fixed on their boundaries, but allow arbitrary chemical occupancy of the interior sites. Replacing 20% of NiNi pairs with AlCo pairs eliminates all bow-tie tiles from the minimum-energy configuration and leads to chemical composition $\text{Al}_{0.720}\text{Ni}_{0.166}\text{Co}_{0.114}$, still within the limits of the basic Ni composition. The low-energy configurations consist entirely of HBS tiles decorated as found previously, but now many tile edges that participate in two 72° junctions get decorated with an AlCo pair rather than a NiNi pair [see Fig. 4(b)].

IV. COMPARISON

We compare our model with structural models based on several recent experiments. *Z*-contrast electron microscope imagery⁵ images atomic columns proportionally to the mean-square atomic number of the column, so the images translate quite directly into TM positions. A key feature of the experimental data is the occurrence of decagonal rings with 20 Å diameter. These rings exhibit up to ten TM doublets around the perimeter, an interior ring of ten TM singlets, and a central triangular core.⁵ This characteristic structure is in excellent agreement with our model, where two hexagons and a boat frequently coalesce into a decagonal cluster [see center of Fig. 4(b)]. The triangular core of this cluster, which breaks decagonal symmetry, is recognized as the sail of the boat tile. Full *ab initio* calculations¹⁴ recently verified energetic favorability of this particular core structure.¹⁵

One disagreement between our work and the *Z*-contrast imagery is that we find a lower apparent density of complete 20 Å decagonal rings. It is conceivable that phason stacking disorder (tilings differ in adjoining 4 Å slabs by localized bow-tie flips) increases the apparent density of decagonal rings.¹⁶ Alternatively, partial TM occupancy may be responsible as discussed in connection with our defect tile.

We can also compare our results with recent structure refinements based on x-ray data sets. The refinements by Takakura *et al.*⁶ and by Cervellino *et al.*⁷ resemble our model in several key respects. In particular, both feature fre-

quent TM doublets along HBS tile edges. Polarized extended x-ray absorption fine-structure experiments¹⁷ (EXAFS) confirm that Co atoms are isolated from other TM atoms, and Ni atoms do have Ni neighbors at positions consistent with our edge decoration model. Sites where the Al atoms of AlCo pairs replace NiNi pairs in our model are among the sites where x-ray data indicate partial TM occupancy (specifically Al/TM mixing on orbits 6 and 7 in Ref. 6, and partial Ni occupancy in Ref. 7).

In fact, the partial TM occupancy or AlTM mixing is more prevalent in the structure refinements^{6,7} than in our model, even at the reduced Ni composition. This may be a finite temperature effect in the real materials, while our modeling effort discussed here concerns minimum-energy states. Indeed, we do find AlTM mixing at elevated temperatures. Additionally, increasing the atomic volume by reducing the total density will cause significant partial occupancy.

Another small difference between our model and the experimental refinements is the asymmetric placement of interior Al atoms in the S and B supertiles. These are the two Al atoms closest to the central Co in the small 2.45 Å edge length S tiles that are contained within the S and B supertiles. Takakura *et al.*⁶ find the occupied sites lie at positions (their orbit 23) rotated by 36° from our positions (their orbit 10), while Cervellino *et al.*⁷ find them at both types of positions, within the “puckered” layers. In our simulations the alternate positions are energetically unfavorable, although they become favorable after small relaxations of the atoms at those positions.

Our study began with interatomic potentials plus a minimum of experimental information. We derived structural models starting with a minimally constrained lattice gas on a fluctuating rhombus tiling. Systematically removing unnecessary degrees of freedom yielded a nearly deterministic decoration of HBS tiles at a length scale τ^2 times larger than the initial rhombus tiling, a model consistent with *Z*-contrast electron microscopy and x-ray diffraction. This procedure can be repeated to identify yet larger characteristic atomic clusters providing an example of multiscale modeling that might be applicable to other quasicrystals.

ACKNOWLEDGMENTS

This research was supported in part by the National Science Foundation Grant No. DMR-0111198 at Carnegie Mellon University and by DOE Grant No. DE-FG02-89ER-45405 at Cornell. Part of this work was performed under the auspices of the U.S. Department of Energy at Lawrence Livermore Laboratory under Contract No. W-7405-ENG-48. We acknowledge useful discussions with W. Steurer, A. Cervellino, H. Takakura, E. Abe, P.J. Steinhardt, and S.J. Pennycook.

¹S. Ritsch, C. Beeli, H.-U. Nissen, T. Godecke, M. Scheffer, and R. Luck, *Philos. Mag. Lett.* **78**, 67 (1998).

²S. Ritsch, C. Beeli, H.-U. Nissen, T. Godecke, M. Scheffer, and R. Luck, *Philos. Mag. Lett.* **74**, 99 (1996); A.P. Tsai, A.

Fujiwara, A. Inoue, and T. Masumoto, *ibid.* **74**, 233 (1996).

³W. Steurer, T. Haibach, B. Zhang, S. Kek, and R. Lück, *Acta Crystallogr., Sect. B: Struct. Sci.* **B49**, 661 (1993).

⁴A. Yamamoto and S. Weber, *Phys. Rev. Lett.* **78**, 4430 (1997); P.J.

- Steinhardt, H.-C. Jeong, K. Saitoh, M. Tanaka, E. Abe, and A.P. Tsai, *Nature (London)* **396**, 55 (1998); M. Krajčí, J. Hafner, and M. Mihalkovič, *Phys. Rev. B* **62**, 243 (2000).
- ⁵E. Abe, K. Saitoh, H. Takakura, A.P. Tsai, P.J. Steinhardt, and H.-C. Jeong, *Phys. Rev. Lett.* **84**, 4609 (2000); Y. Yan, S.J. Pennycook, and A.P. Tsai, *ibid.* **81**, 5145 (1998).
- ⁶H. Takakura, A. Yamamoto, and A.-P. Tsai, *Acta Crystallogr., Sect. A: Found. Crystallogr.* **A57**, 576 (2001).
- ⁷A. Cervellino, T. Haibach, and W. Steurer (unpublished).
- ⁸J.A. Moriarty and M. Widom, *Phys. Rev. B* **56**, 7905 (1997); M. Widom and J.A. Moriarty, *ibid.* **58**, 8967 (1998); M. Widom, I. Al-Lehyani, and J.A. Moriarty, *ibid.* **62**, 3648 (2000).
- ⁹I. Al-Lehyani, M. Widom, Y. Wang, N. Moghadam, G.M. Stocks, and J.A. Moriarty, *Phys. Rev. B* **64**, 075109 (2001).
- ¹⁰C. L. Henley, *Random Tiling Models in Quasicrystals: The State of the Art*, edited by D.P. DiVincenzo and P. J. Steinhardt (World Scientific, Singapore, 1991), p. 429, and references therein.
- ¹¹E. Cockayne and M. Widom, *Phys. Rev. Lett.* **81**, 598 (1998).
- ¹²W. Steurer, *Mater. Sci. Eng., A* **294-296**, 268 (2000).
- ¹³S.E. Burkov, *Phys. Rev. Lett.* **67**, 614 (1993).
- ¹⁴Y. Yan and S.J. Pennycook, *Phys. Rev. Lett.* **86**, 1542 (2001).
- ¹⁵The overlap rules described in Ref. 14 are not sufficient by themselves to force perfect quasiperiodicity.
- ¹⁶C.L. Henley, V. Elser, and M. Mihalkovic, *Z. Kristallogr.* **215**, 553 (2000).
- ¹⁷O. Zaharko, C. Menebhini, A. Cervellino, and E. Fischer, *Eur. Phys. J. B* **19**, 5273 (2001).